Supplement of Clim. Past, 16, 227–243, 2020
https://doi.org/10.5194/cp-16-227-2020-supplement

Climate of the Past
Open Access
EGU

Supplement of

Alluvial record of an early Eocene hyperthermal within the Castissent Formation, the Pyrenees, Spain

Louis Honegger et al.

Correspondence to: Louis Honegger (louis.honegger@unige.ch)

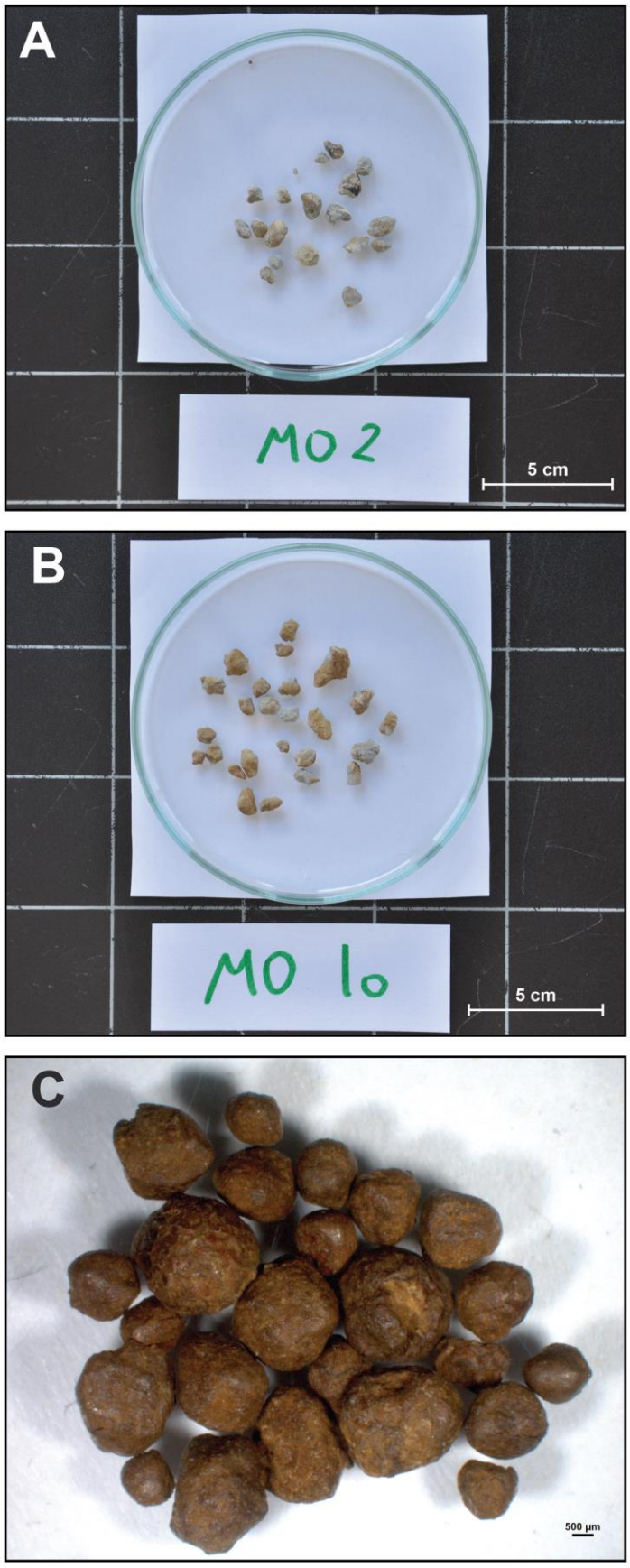

Figure S1: Macroscopic view of pedogenic nodules from the Chiriveta section. A and B show carbonate nodules from samples MO2 ans MO10 respectively. C shows iron-oxide and hydroxides nodules from sample RB3-4.

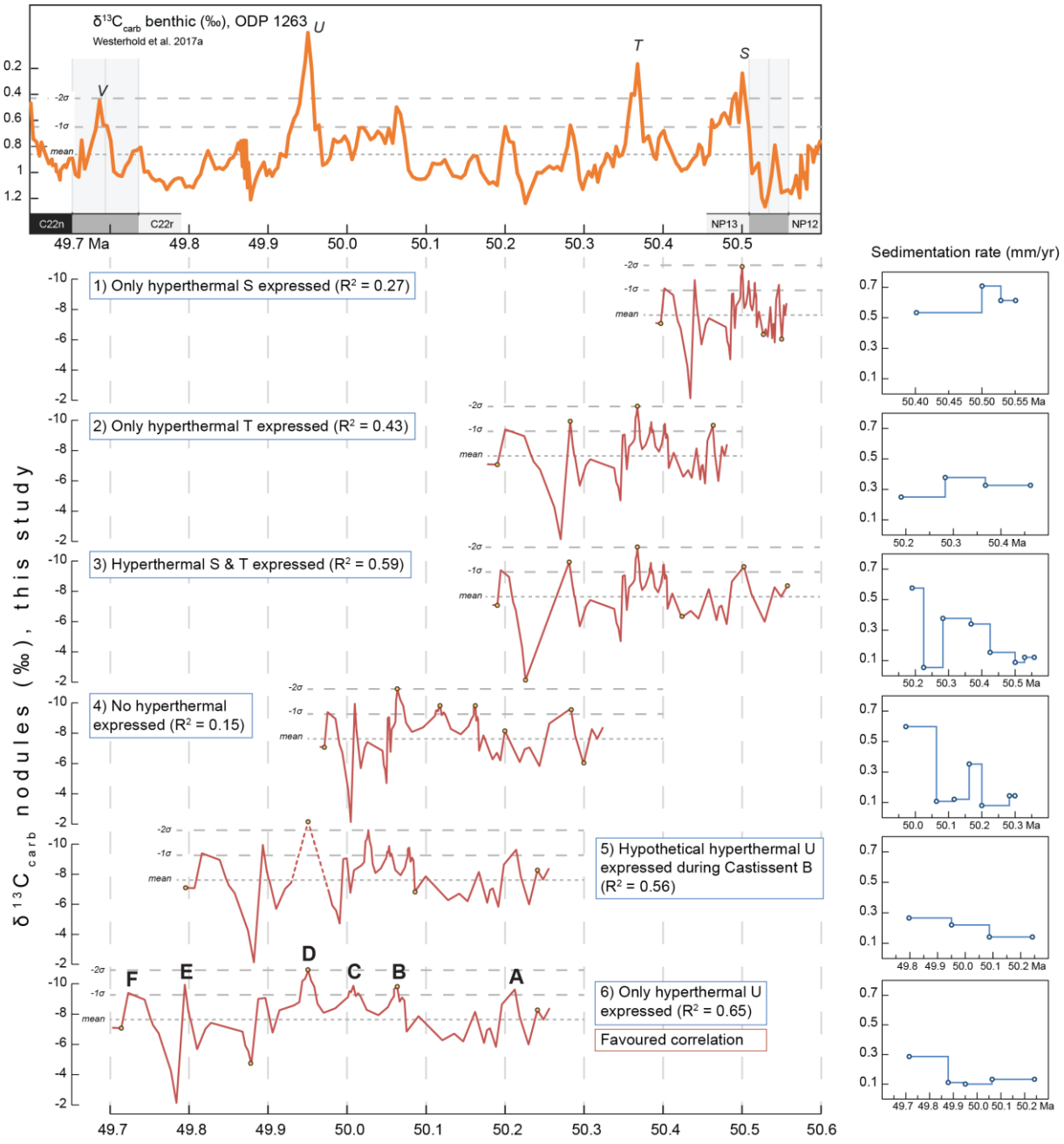

Figure S2: Correlation options 1 to 6 between $\delta^{13}C$ benthic record from site 1263 and $\delta^{13}C$ from carbonate nodules (this study) using the Analyseries software (Paillard et al., 1996). Tie-points used to correlate both curves are showed in yellow dots. Sedimentation rate in mm/yr for each option is showed on the right. Option 6 is detailed in Figure 7.

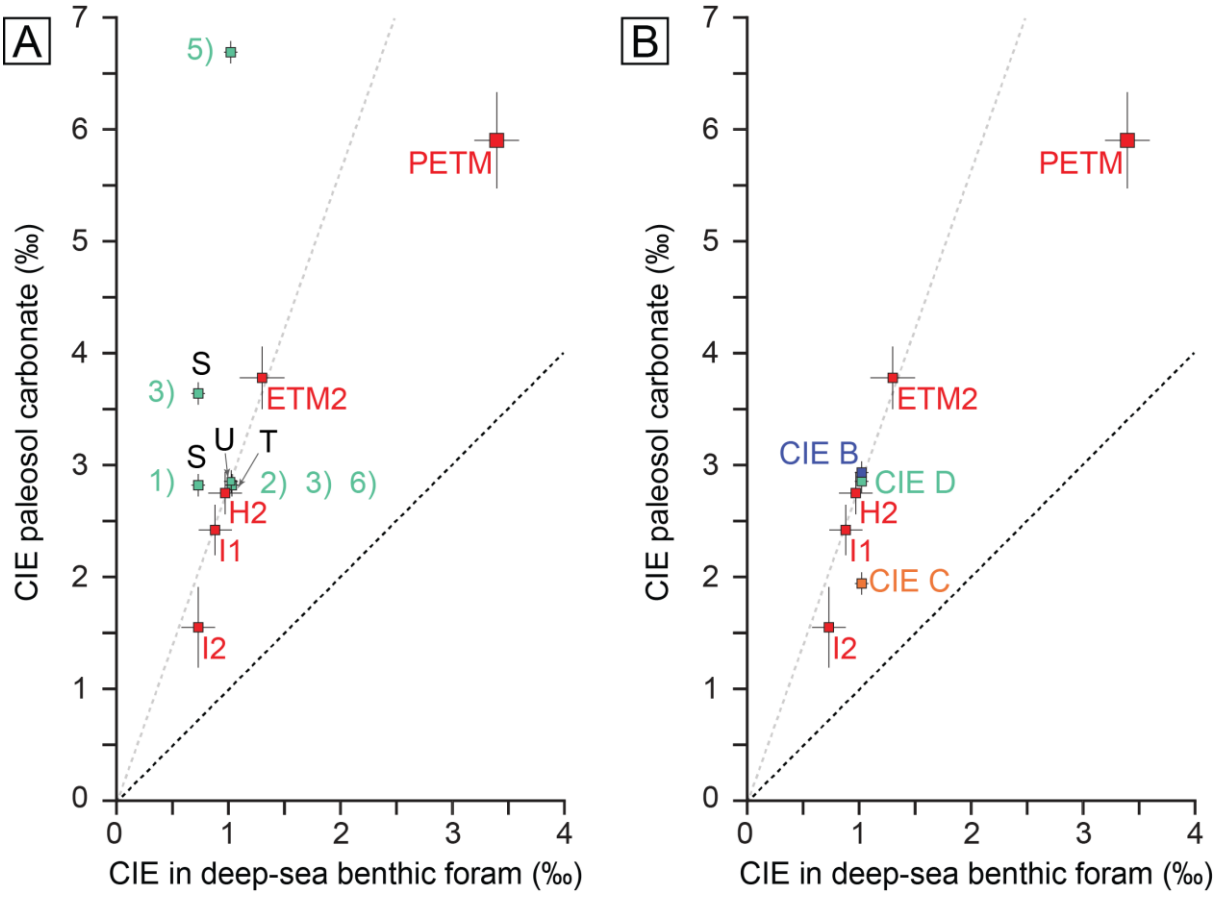

Figure S3: CIE amplitudes from I1, I2, H2, ETM2 and PETM in continental and marine environments after (Abels et al., 2016). A - Options 1 to 6 from Figure S2 are plotted as comparison. B – CIE B, C and D from option 6 are plotted as comparison.

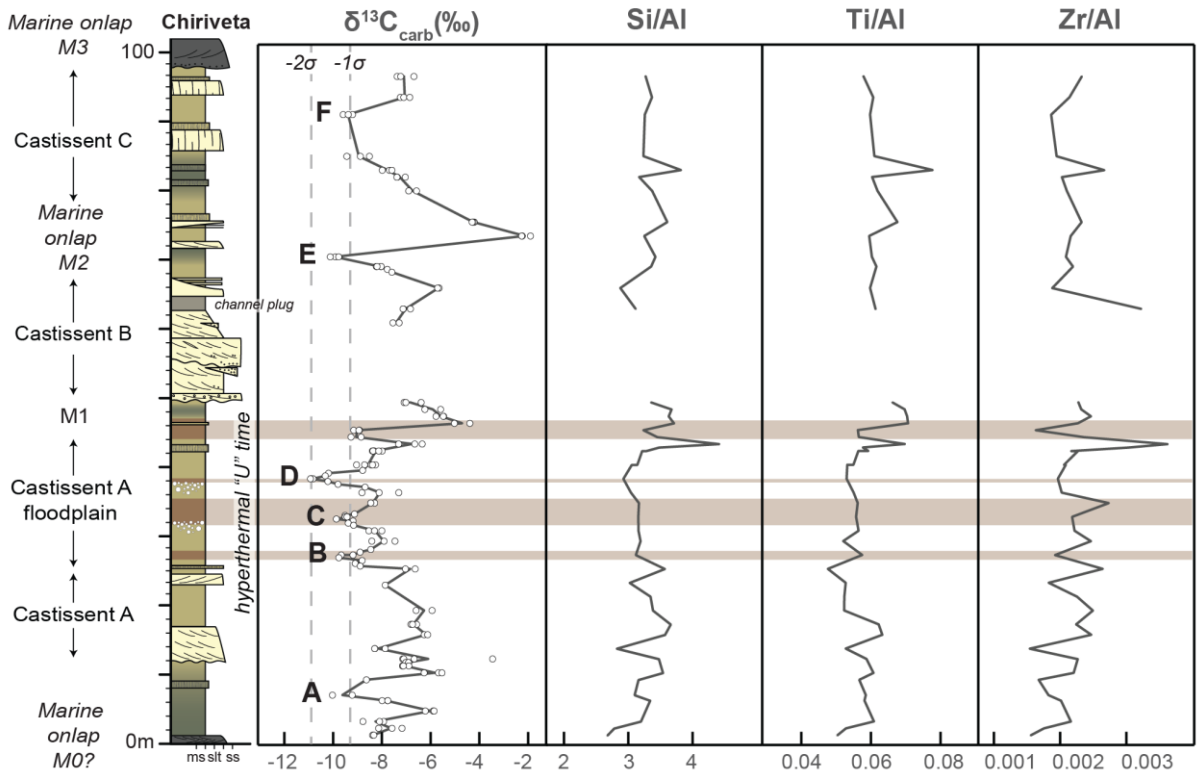

Figure S4: Chiriveta section showing $\delta^{13}C$ and grain-size proxies Si/Al, Ti/Al and Zr/Al. Al is more concentrated in the fines and Si, Ti and Zr in the coarse fraction of the sediment (Lupker et al., 2012). An increase of these ratios would suggest an increase in grain-size. Here, no direct correlation is observable between the grain size and the CIEs.

Sample Name	D50(um)	Mean channel h (m)	Holbrook Slope	Trampush Slope
CH1	309.4	3.75	0.00025	0.00025
CH2	510.2	3.75	0.00042	0.00029
CH3	400.6	3.75	0.00033	0.00027
CH4	466.6	3.75	0.00038	0.00028
CH5	403.2	3.75	0.00033	0.00027
CH6	635.9	3.75	0.00052	0.00030
CH7	332.2	3.75	0.00027	0.00026
CH8	377.4	3.75	0.00031	0.00027
CH10	241.8	3.75	0.00020	0.00024
CH11	174.2	3.75	0.00014	0.00022
CH12	20.4	3.75	0.00002	0.00013
CH13	33.4	3.75	0.00003	0.00014
CH14	24.0	3.75	0.00002	0.00013
CH15	21.1	3.75	0.00002	0.00013

Table S1: D50 values for 14 samples of the Chiriveta section. Analyses were carried using a Bettersizer S3 Plus. Approximately 70'000 grains were analysed by sample. Holbrook and Wanas, (2014) and Trampush et al. (2014) equations were used to calculate the paleoslope.

Sample	Phyllos	Quartz	Fsp-K	Plg-Na	Calcite	Indosés	Smectite	Ill-Sme	Mica	Chlorite	Kaolinite
MO2	35.30	23.38	0.00	1.12	36.08	2.01	38.06	3.82	29.97	15.47	12.69
MO3	50.32	33.98	1.88	1.77	6.83	0.72	34.67	3.16	34.87	19.85	7.45
MO4	21.58	15.75	0.00	0.00	53.96	8.71	31.04	2.42	24.12	20.31	22.12
MO5	13.71	19.59	0.00	0.00	62.52	1.84	26.73	5.86	20.79	33.84	12.78
MO6	34.78	27.56	1.77	0.00	30.23	1.19	38.81	1.38	20.87	30.41	8.53
MO7	32.57	39.76	3.08	1.03	20.56	3.00	26.97	2.93	32.95	29.87	7.28

Table S2: Clay minerals results from sample MO2 to MO7 in the top of the Castissent Formation Member A, between 44 and 50m. From (Nicolaides, 2017).

sample	height (m)	Age (kyrs)	Al (%)	Ti (%)	Zr (ppm)	MAP
2CH21	96	49703.7	3.04	0.18	71	185
2CH20	93	49714.2	4.81	0.29	103	304
2CH19	90.5	49722.9	5.70	0.34	106	360
2CH18	84.5	49743.9	6.47	0.39	126	402
2CH17	82.5	49750.9	4.45	0.35	119	334
2CH16	81.5	49754.4	5.73	0.35	116	355
2CH15	79.5	49761.4	5.43	0.34	114	339
S093	75	49777.1	3.20	0.22	74	222
S092	73	49784.1	3.11	0.19	67	221
S091	70	49794.6	7.81	0.47	163	648
S090	68.6	49799.4	6.14	0.38	135	403
S089	65.5	49810.3	4.69	0.28	88	274
S088	62.5	49820.8	6.07	0.37	196	395
MO2	49	49867.9	5.18	0.34	118	341
MO3	48	49871.4	7.32	0.51	170	568
MO4	47	49874.9	3.33	0.23	82	226
MO5	46	49878.7	3.03	0.21	69	199
MO6	45	49887.7	6.20	0.35	101	394
MO7	44	49896.7	6.86	0.39	162	451
MO8	43	49905.7	3.55	0.25	129	264
MO9	42.5	49910.2	5.59	0.32	169	351
MO10	42	49914.7	6.54	0.39	142	417
CH13	42	49914.7	7.18	0.40	163	433
MO11	40	49932.6	7.15	0.39	147	447
CH12	40	49932.6	6.54	0.35	136	367
CH11	38	49950.6	8.96	0.47	176	491
CH10	36	49970.4	7.03	0.39	142	399
CH9	34.5	49985.3	6.75	0.38	185	414
CH8	32.5	50005.1	9.35	0.52	204	754
CH7	30.5	50025.0	5.89	0.33	131	352
CH6	29	50039.8	5.97	0.31	147	359
CH5	27	50059.7	8.62	0.50	166	604
CH4	25	50075.5	6.39	0.30	169	409
CH3	23	50090.6	8.48	0.45	155	515
CH2	21	50105.7	6.85	0.36	155	420
CH1	19	50120.7	6.38	0.33	159	388
2CH14	17	50135.8	5.63	0.35	126	373
2CH13	15.5	50147.0	5.57	0.35	138	361
2CH12	13.5	50162.1	6.18	0.33	95	349
2CH11	12	50173.4	4.15	0.24	94	260
2CH10	10	50188.4	4.74	0.29	104	298
2CH9	9	50196.0	6.19	0.35	104	382
2CH8	6.8	50212.5	6.99	0.41	128	435
2CH7	6	50218.5	5.16	0.30	104	317
2CH6	3	50241.1	4.22	0.26	91	263
2CH5	2	50248.6	4.67	0.25	82	283
2CH4	1	50256.2	5.63	0.28	88	334

sample	height (m)	Age (kyrs)	$\delta^{13}C$ ‰ VPDB	$\delta^{18}O$ ‰ VPDB	
2CH21-P1	96	49703.7	-7.4	-5.2	
2CH21-P2	96	49703.7	-7.2	-5.0	
2CH21-G3	96	49703.7	-6.7	-6.1	
2CH20-P1	93	49714.2	-7.2	-6.3	
2CH20 P2	93	49714.2	-7.1	-5.4	
2CH20-G3	93	49714.2	-6.9	-5.5	
2CH19-P1	90.5	49722.9	-9.2	-5.7	
2CH19-G2	90.5	49722.9	-9.6	-5.7	
2CH19-G3	90.5	49722.9	-9.4	-5.7	
2CH18-P1	84.5	49743.9	-8.5	-6.1	
2CH18-P2	84.5	49743.9	-9.4	-5.9	
2CH18-P3	84.5	49743.9	-8.9	-6.0	
2CH17-P1	82.5	49750.9	-7.7	-6.3	
2CH17-P2	82.5	49750.9	-8.0	-6.2	
2CH17-G3	82.5	49750.9	-7.6	-6.4	
2CH16-P1	81.5	49754.4	-7.4	-6.5	
2CH16-P2	81.5	49754.4	-7.0	-6.2	
2CH16-G3	81.5	49754.4	-7.4	-6.4	
2CH15-P1	79.5	49761.4	-6.9	-6.5	
2CH15-P2	79.5	49761.4	-6.6	-6.6	
93-P1	75	49777.1	-4.2	-6.1	
93-P2	75	49777.1	-4.3	-6.1	
93-P3	75	49777.1	-4.3	-6.3	
92-P1	73	49784.1	-1.9	-6.4	
92-P2	73	49784.1	-2.2	-6.4	
92-P3	73	49784.1	-2.3	-6.4	
91-P1	70	49794.6	-9.9	-5.7	
91-P2	70	49794.6	-10.1	-6.0	
91-G3	70	49794.6	-9.8	-6.3	
90-P1	68.6	49799.4	-8.0	-6.1	
90-P2	68.6	49799.4	-8.0	-6.1	
90-P3	68.6	49799.4	-8.2	-6.0	
RB4-3	68.6	49799.4	-8.2	-5.5	
RB4-2	68.2	49799.4	-7.8	-6.0	
RB4-1	67.8	49800.8	-7.6	-6.3	
89-P1	65.5	49810.3	-5.7	-6.3	
89-P2	65.5	49810.3	-5.7	-6.4	
88-P1	62.5	49820.8	-6.8	-6.2	
88-G2	62.5	49820.8	-7.1	-6.1	
88-G3	62.5	49820.8	-7.1	-6.2	
87-P1	60.5	49827.7	-7.5	-6.5	
87-P2	60.5	49827.7	-7.3	-6.4	
MO2-P1	49	49867.9	-7.1	-5.6	
MO2-P2	49	49867.9	-7.0	-5.7	
MO2-P3	49	49867.9	-6.4	-5.8	
MO3-P1	48	49871.4	-5.6	-6.0	
MO3-P2	48	49871.4	-6.2	-5.8	
MO4-P1	47	49874.9	-5.8	-5.1	
MO4-P2	47	49874.9	-5.5	-5.1	
MO4-P3	47	49874.9	-5.5	-5.2	

sample	height (m)	Age (kyrs)	$\delta^{13}C$ ‰ VPDB	$\delta^{18}O$ ‰ VPDB	
MO5-G1	46	49878.7	-4.4	-6.3	
MO5-G2	46	49878.7	-5.0	-6.2	
MO6-P1	45	49887.7	-9.2	-5.6	
MO6-P2	45	49887.7	-8.9	-5.7	
MO6-P3	45	49887.7	-8.9	-5.6	
MO7-P1	44	49896.7	-8.9	-5.2	
MO7-P2	44	49896.7	-9.3	-5.3	
MO8-P1	43	49905.7	-7.3	-5.9	
MO8-P2	43	49905.7	-6.7	-5.9	
MO8-G3	43	49905.7	-6.3	-6.0	
MO10-P1	42	49914.7	-8.3	-5.9	
MO10-P2	42	49914.7	-8.3	-6.1	
MO10-P3	42	49914.7	-8.4	-6.0	
CH13-P3	42	49914.7	-8.0	-5.8	
CH13-P2	42	49914.7	-8.4	-5.9	
CH13-P1	42	49914.7	-8.1	-5.4	
MO11-P1	40	49932.6	-8.5	-5.6	
MO11-P2	40	49932.6	-8.3	-5.9	
CH12-P3	40	49932.6	-8.7	-5.3	
CH12-P2	40	49932.6	-8.4	-5.8	
CH12-P1	40	49932.6	-9.0	-5.2	
RB3-7	39.2	49939.8	-8.8	-6.1	
RB3-6	38.8	49943.4	-10.2	-5.9	
RB3-5	38.4	49947.0	-10.3	-5.9	
RB3-4B	38	49950.6	-10.8	-5.9	
RB3-4A	38	49950.6	-10.9	-5.8	
RB3-3	37.6	49954.6	-10.2	-6.0	
RB3-2	37.2	49958.5	-9.8	-6.3	
RB3-1	36.8	49962.5	-8.7	-6.3	
CH10-G3	36	49970.4	-7.3	-6.2	
CH10-P2	36	49970.4	-8.1	-6.0	
CH10-P1	36	49970.4	-8.8	-5.9	
CH9-P2	34.5	49985.3	-8.3	-6.1	
CH9-P1	34.5	49985.3	-8.5	-6.4	
RB2-7	32.9	50001.2	-9.1	-6.5	
RB2-6	32.7	50003.1	-9.5	-6.1	
RB2-5B	32.5	50005.1	-9.5	-6.2	
RB2-5A	32.5	50005.1	-9.4	-6.0	
RB2-4	32.2	50008.1	-9.9	-5.8	
RB2-3	31.9	50011.1	-9.2	-6.0	
RB2-2	31.6	50014.1	-9.4	-5.8	
RB2-1	31.3	50017.0	-9.2	-5.8	
CH7-P3	30.5	50025.0	-8.5	-5.9	
CH7-P2	30.5	50025.0	-8.0	-6.0	
CH7-P1	30.5	50025.0	-8.3	-6.0	
CH6-P3	29	50039.8	-8.4	-6.1	
CH6-P2	29	50039.8	-7.5	-6.2	
CH6-G1	29	50039.8	-7.9	-6.0	
RB1-7	27.8	50051.7	-8.5	-6.8	

sample	height (m)	Age (kyrs)	$\delta^{13}C$ ‰ VPDB	$\delta^{18}O$ ‰ VPDB	
RB1-6	27.4	50055.7	-8.9	-6.8	
RB1-5B	27	50059.7	-9.2	-6.1	
RB1-5A	27	50059.7	-9.7	-6.0	
RB1-4	26.6	50063.5	-9.8	-6.0	
RB1-3	26.2	50066.5	-8.8	-6.2	
RB1-2	25.8	50069.5	-9.1	-6.3	
RB1-1	25.4	50072.5	-8.9	-5.9	
CH4-P2	25	50075.5	-6.6	-6.5	
CH4-P1	25	50075.5	-7.0	-6.2	
CH3-P1	23	50090.6	-7.9	-5.3	
CH1-P2	19	50120.7	-5.9	-6.1	
CH1-P1	19	50120.7	-6.6	-6.0	
2CH14-P1	17	50135.8	-6.6	-5.7	
2CH14-P2	17	50135.8	-6.8	-5.8	
2CH14-P3	17	50135.8	-6.7	-5.6	
2CH13-P1	15.5	50147.0	-6.3	-6.5	
2CH13-P2	15.5	50147.0	-6.1	-6.7	
2CH12-P1	13.5	50162.1	-8.3	-5.3	
2CH12-P2	13.5	50162.1	-8.3	-5.4	
2CH12-G3	13.5	50162.1	-7.9	-5.4	
2CH3-P1	12	50173.4	-3.5	-7.0	
2CH11-P1	12	50173.4	-7.1	-5.9	
2CH11-P2	12	50173.4	-6.7	-5.9	
2CH11-G3	12	50173.4	-7.1	-5.8	
2CH1-P1	11.5	50177.1	-6.9	-5.5	
2CH1-P2	11.5	50177.1	-7.0	-5.5	
2CH1-P3	11.5	50177.1	-6.9	-5.5	
2CH2-P1	11	50180.9	-7.2	-5.5	
2CH2-P2	11	50180.9	-6.9	-5.5	
2CH2-P3	11	50180.9	-7.1	-5.7	
2CH10-P1	10	50188.4	-5.7	-6.6	
2CH10-P2	10	50188.4	-5.5	-6.6	
2CH10-G3	10	50188.4	-6.3	-6.6	
2CH9-P1	9	50196.0	-8.6	-5.5	
2CH8-P1	6.8	50212.5	-10.0	-5.1	
2CH8-P2	6.8	50212.5	-9.2	-5.3	
2CH7-P1	6	50218.5	-8.0	-5.9	
2CH7-P2	6	50218.5	-7.8	-5.8	
2CH7-G3	6	50218.5	-7.8	-5.7	
2CH6BIS-P1	4.5	50229.8	-5.9	-6.5	
2CH6BIS-P2	4.5	50229.8	-6.2	-6.4	
2CH6BIS-P3	4.5	50229.8	-5.9	-6.6	
2CH6-P1	3	50241.1	-7.9	-6.3	
2CH6-P2	3	50241.1	-8.8	-6.2	
2CH6-G3	3	50241.1	-8.1	-6.3	
2CH5-P1	2	50248.6	-7.6	-6.3	
2CH5-P2	2	50248.6	-8.1	-6.2	
2CH5-P3	2	50248.6	-7.2	-6.3	
2CH4-P1	1	50256.2	-8.4	-6.1	
2CH4-P2	1	50256.2	-8.3	-6.3	

Table S3: Al, Ti, Zr, MIA, δ13C and δ18O values of the Chiriveta section.

Age from correlation in Fig. 7

height Chiriveta (m)	age 1263 (kyrs)
93.0	49714.1
46.1	49878.2
38.0	49950.6
26.7	50063.1
2.9	50241.5

Table S4 : Correlation pointers between age of ODP site 1263 and Chiriveta's section height

References Supplement

Abels, H. A., Lauretano, V., van Yperen, A. E., Hopman, T., Zachos, J. C., Lourens, L. J., Gingerich, P. D. and Bowen, G. J.: Environmental impact and magnitude of paleosol carbonate carbon isotope excursions marking five early Eocene hyperthermals in the Bighorn Basin, Wyoming, Clim. Past, 12, 1151–1163, doi:10.5194/cp-12-1151-2016, 2016.

Holbrook, J. and Wanas, H.: A Fulcrum Approach To Assessing Source-To-Sink Mass Balance Using Channel Paleohydrologic Paramaters Derivable From Common Fluvial Data Sets With An Example From the Cretaceous of Egypt, J. Sediment. Res., 84, 349–372, doi:10.2110/jsr.2014.29, 2014.

Lupker, M., France-Lanord, C., Galy, V., Lavé, J., Gaillardet, J., Gajurel, A. P., Guilmette, C., Rahman, M., Singh, S. K. and Sinha, R.: Predominant floodplain over mountain weathering of Himalayan sediments (Ganga basin), Geochim. Cosmochim. Acta, 84, 410–432, doi:10.1016/j.gca.2012.02.001, 2012.

Nicolaides, E.: Analyses des sédiments marins et continentaux éocènes dans les Pyrénées Espagnoles, BSc Thesis, Université de Lausanne., 2017.

Paillard, D., Labeyrie, L. and Yiou, P.: Macintosh Program performs time-series analysis, Eos, Trans. Am. Geophys. Union, 77, 379–379, doi:10.1029/96eo00259, 1996.

Trampush, S. M., Huzurbazar, S. and Mcelroy, B.: Empirical assessment of theory for bankfull, Water Resour. Res., 50, 9211–9220, doi:10.1002/2014WR015597.Received, 2014.